Journal of Applied Geophysics 220 (2024) 105272

Contents lists available at ScienceDirect

Journal of Applied Geophysics

journal homepage: www.elsevier.com/locate/jappgeo

Unveiling a hidden fortification system at "Faraglioni" Middle Bronze Age Village of Ustica Island (Palermo, Italy) through ERT and GPR prospections

Anna Russolillo [a,b], Franco Foresta Martin [c,d], Antonio Merico [e], Vincenzo Sapia [d,*], Pierfrancesco Talamo [f], Valerio Materni [d], Marta Pischiutta [d], Sandro de Vita [d], Stefano Furlani [g], Domenico Targia [h], Mauro A. Di Vito [d]

[a] Università degli Studi Suor Orsola Benincasa di Napoli, Italy
[b] Associazione Villaggio Letterario, Ustica, Palermo, Italy
[c] Laboratorio Museo di Scienze della Terra, Ustica, Palermo, Italy
[d] Istituto Nazionale di Geofisica e Vulcanologia, Italy
[e] Università degli Studi di Siena, Italy
[f] Ministero dei Beni Culturali, Italy
[g] Dipartimento di Matematica e Geoscienze, Università di Trieste, Italy
[h] Regione Siciliana, Parco Archeologico di Himera, Solunto e Monte Iato, Italy

ARTICLE INFO

Keywords:
Georadar
Electrical resistivity tomography
Middle Bronze Age
Villaggio Dei Faraglioni
Fortification system
Ustica Island

ABSTRACT

We carried out a geophysical research project in the Middle Bronze Age village of Ustica (Palermo, Sicily, Italy), named "Faraglioni Village" after the stack formations which detach from the coast north of the archaeological site. The investigation, which comprised Electrical Resistivity Tomography (ERT) and Ground Penetrating Radar (GPR) techniques, allowed us to discover the buried foundations of an outwork fortification system never evidenced by previous archaeological studies, only hypothesised from the observation of aerial photography and partially outcropping boulders, which align roughly parallel to the main defensive wall of the Village.

Our geophysical prospection involved the entire 250 m-long arc of the outward village defensive wall, with the acquisition of eleven ERT profiles and 27 GPR scans. The techniques were selected based on both favourable logistics and methods applicability: ERT sections allowed us to trace a series of high-resistivity anomalies arranged to form an arc-shaped structure along the perimeter of the defensive wall. GPR investigation was localised in the most accommodating patch of terrain of the site, with the effort of intercepting clear enough sections of the target, to determine more accurately its shape, depth, and overall dimensions. Our discovery paves the way for new investigations, mainly aimed at defining the timing of construction of the fortification system, as well as the function of the remains of other architectural structures identified close to the wall, which could represent the target of further geophysical investigations.

1. Introduction

The "Faraglioni Village" is a Middle Bronze Age settlement located on the northern coast of the volcanic island of Ustica (Palermo, Sicily, Italy). It was built on a coastal terrace boarded by high sea cliffs and protected on the landward side by a long and massive arched wall, strengthened by buttresses. Its current ruins cover an area of about 7000 m2, where dozens of drywall masonry structures flanked by narrow streets have been unearthed. Several archaeological campaigns conducted at the site by different teams since the 1970s have highlighted a complex and multi-functional use of space and recovered abundant and well-preserved household goods, mostly pottery (Mannino, 1970, 1979, 1982; Holloway and Lukesh, 1995, 2001; Spatafora, 2016; Spatafora et al., 2008; Foresta Martin and Frurlani, 2021). Despite its monumentality, the defense system of this settlement has been so far poorly investigated, and several aspects about it, including its general layout, construction technique, chronology and function need to be deepened and clarified (Russolillo et al., 2022). To fill this gap of knowledge, we performed a multi-parametric geophysical prospection, thorough a layout of Electrical Resistivity Tomography (ERT) and Ground

* Corresponding author at: INGV, Italy.
E-mail address: vincenzo.sapia@ingv.it (V. Sapia).

https://doi.org/10.1016/j.jappgeo.2023.105272
Received 27 May 2023; Received in revised form 15 November 2023; Accepted 12 December 2023
Available online 16 December 2023

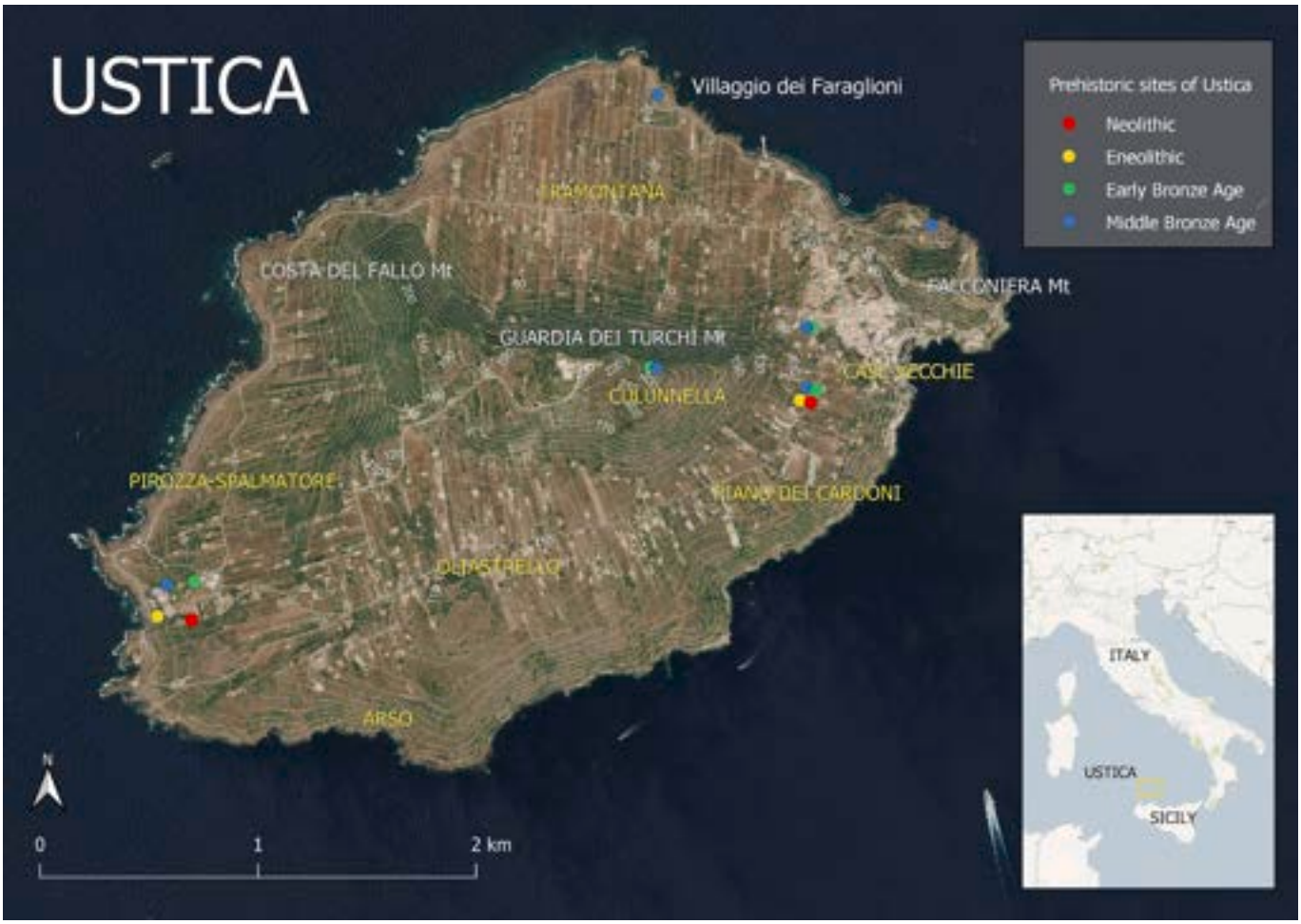

Fig. 1. The island of Ustica (Sicily, Italy) with the indication of the main reliefs and plains. The colored dots mark the phases of the main prehistoric settlements.

Penetrating Radar (GPR) profiles, which are consolidated geophysical methods in archaeological context and constitute a valid tool for the non-invasive recovery of subsurface information (Neubauer et al., 2002; Orlando et al., 2019; Porcelli et al., 2020; Corradini et al., 2020, 2022). The combined use of such methodologies have proven to be especially effective, as they offer a way to interpret subsurface data more robustly (Di Mauro et al., 2014; Balkaya et al., 2021; Akca et al., 2019; Yilmaz et al., 2019; Sapia et al., 2021; Balkaya et al., 2021), since the different sets of physical properties exploited by each methodology can be compared and either strengthen or exclude hypotheses about the anomalies recovered.

Fortifications and fortified settings have been reportedly studied with geophysical techniques (Epimakhov et al., 2016; Milo et al., 2022; Murín et al., 2022), yielding interesting conclusions, some of which we adopted in our work to guide the interpretation and representation of the data from "Faraglioni Village". For instance, from Milo et al. of 2022, which is set to investigate a geological context quite different from our study area, magnetic measurements proved to be very effective, while they would result impractical in this study, since the volcanic (strongly ferromagnetic) materials constituting both the subsoil and the researched targets would not offer enough contrast for subsurface imaging. On the contrary, ERT investigation proved to be successful and yielded some comprehensive information about the near-surface, not only revealing the uppermost geological asset of the site, but also rendering clear traces of the researched anthropological targets.

In this work, geophysical measurements were concentrated along a land-strip outside the main defensive wall, where 0.3–1 m large rows of boulders emerge discontinuously from the ground. The main goal was to further investigate whether this path, trending nearly-parallel to the main wall at 6–7 m distance, may correspond to a second wall structure at depth. The evidence gathered thanks to our geophysical campaign allowed us not only to validate our former assumption, but in addition they suggest new hints and considerations to the complex picture of the defensive system characterising this settlement. As for GPR data, we managed to extract data which we consider complementary to that from ERT; we feel that this is the actual strength of combined geophysical prospections: we used one technique to map the location on a larger scale, while completing the investigation with a set of acquisitions focused on a smaller yet representative sector of the site.

2. Ustica in space and time

2.1. Geographic and geological outline

Ustica is a small volcanic island (8,6 km^2) located in the Southern Tyrrhenian Sea, about 65 km to the north of Palermo, Sicily, Italy (Fig. 1). Its origin dates back to the middle Pleistocene, about one million years ago, when the expansion of the Tyrrhenian basin opened deep crustal faults, causing the rise of magma from the upper mantle, and the formation of a volcanic seamount off the northwestern coast of Sicily (Barberi et al., 1969; Barberi and Innocenti, 1980; de Vita, 1993; de Vita et al., 1998).

For about half a million years the volcanic activity was submarine, and subsequently it became subaerial, leading to the emergence of an island with several eruptive centers, characterised by both effusive and explosive activity. Subaerial volcanic activity lasted for about 400

Fig. 2. The Middle Bronze Age "Faraglioni" village at Ustica and the long and arched defensive wall. (Drone photo by V. Ambrosanio, 2022). Orange rectangle locates the GPR survey while green polygon locates the ERT survey area. (For interpretation of the references to colour in this figure legend, the reader is referred to the web version of this article.)

thousand years and ended about 130 thousand years ago. In the last 350 thousand years, the island shape was also influenced by the eustatic sea level changes, leading to the formation of large marine terraces (Romano and Sturiale, 1971; Cinque et al., 1988; de Vita, 1993; de Vita and Orsi, 1994; de Vita et al., 1995, 1998; de Vita and Foresta Martin, 2017).

The morphology of Ustica is characterised by a median chain of three East-West aligned reliefs which are the relics of volcanic buildings: Monte Guardia dei Turchi in the center (248 m asl); Monte Costa del Fallo to the west (238 m asl); and the Falconiera to the east (157 m asl). They divide the island, the northern sector being occupied by the vast Tramontana plain, the southern one with the plains of Piano dei Cardoni and Oliastrello to the southeast, and Spalmatore to the southwest (Fig. 1).

On the island of Ustica there is no permanent hydrographic network, due to the lack of a subsurface aquifer capable of feeding springs. This lack is due to the particular geological structure of the island, which does not allow the establishment of favourable conditions for the accumulation and emergence of infiltration waters (de Vita, 1993). For this reason, the island has always lacked natural resources of drinking water, except for the small amount dripping from the vaults of some marine and terrestrial caves. Therefore, such modest reserves of drinking water, together with the ones collected during the rains in large water-tanks, were the only reserves available for the survival of the inhabitants, domesticated animals, and agricultural practices in prehistoric and proto-historic times (Foresta Martin and Frurlani, 2021).

2.2. The archaeological framework

During the Neolithic, and up to the Middle Bronze Age (6th - 1st millennium BCE), the island of Ustica experienced multiple colonizations from the Sicilian mainland. It remained continuously inhabited by communities who settled along the coast or inland, depending on several factors, such as the geographical features, available resources, and defense requirements (Spatafora et al., 2008; Mannino and Ailara, 2016; Foresta Martin and Frurlani, 2021).

Our understanding of the prehistoric settlements on Ustica primarily relies on surface discoveries of pottery and stone tools. However, the Villaggio dei Faraglioni stands out as a Middle Bronze Age settlement that has undergone numerous archaeological excavations since the 1970s, revealing its fortified nature. This paragraph provides an overview of the main prehistoric sites identified so far on the island of Ustica (Fig. 1).

It appears that the first Neolithic inhabitants who arrived in Ustica selected the flat summit of Pirozza, a small promontory rising 50 m above sea level in the southwestern sector of Spalmatore, as the location to establish a village (Fig. 1). Abundant ceramic artifacts found at the site allowed the identification of three pottery styles: Stentinello, Trichrome, and Diana, corresponding to the Middle and Late Neolithic phases, covering a period from the 6th to 4th millennium BCE (Mannino,

Fig. 3. Planimetry of the Faraglioni Village with the addition of the aligned boulders (green) emerging on the surface in front of the defensive wall (orange) (Modified after Spatafora, 2016). (For interpretation of the references to colour in this figure legend, the reader is referred to the web version of this article.)

1998, 2015). Another Neolithic site with findings was recently discovered in Piano dei Cardoni, located in the southern hinterland of the island at an altitude of approximately 80 m above sea level. Excavation conducted between 2018 and 2020 unearthed artifacts attributed to the Serra D'Alto and Diana styles, dating from the mid to late 5th millennium BCE (Speciale et al., 2021a, 2021b). Prior to this excavation, the archaeological history of this area relied solely on surface discoveries, which indicated the presence of ceramic fragments in the Conca d'Oro style, dating back to the 4th-3rd millennium BCE (the Eneolithic period), as well as pottery shards from the Middle Bronze Age (Mannino, 1991, 1997; Spatafora et al., 2008; Mannino and Ailara, 2016).

Further upstream from the Piano dei Cardoni settlement, on the eastern slope of Monte Guardia dei Turchi, the archaeologist Mannino (1991) discovered traces of a small prehistoric village together with an adjacent necropolis in the early 1990s. The village was situated along the eastern slopes of Mt. Guardia dei Turchi, at an elevation of 238 m above sea level, covering an artificially leveled area of approximately 2000 square meters, enclosed by defensive boulders (Mannino, 1991). The necropolis, consisting of four rock-cut tombs of the "grotticella" type with well-shaft entrances, was located at a slightly lower altitude (Mannino, 1991; Mannino and Ailara, 2016). Surface findings at both sites included fragments of "impasto," a type of handmade pottery decorated in the style of Capo Graziano (Eolie Islands), allowing them to be dated to the Early Bronze Age (2500–2000 BCE) (Mannino, 1991, 1997; Mannino and Ailara, 2016).

The evidence suggests that Ustica experienced its highest prehistoric population during the Middle Bronze Age, between 1400 and 1200 BCE. During this period, it is believed that the island was home to hundreds of inhabitants spread across multiple settlements. The most significant of these was the fortified Village of the Faraglioni on the northern coast of the island. Ceramic artifacts from the Middle Bronze Age were also discovered in other locations on the island, such as Spalmatore, Omo Morto, and Case Vecchie. However, the exact relationship between these smaller settlements and the contemporary fortified village of the Faraglioni remains still unknown.

3. The "Faraglioni" Middle Bronze Age village

3.1. A terrace overlooking the sea

The Villaggio dei Faraglioni derives its name from two sea stacks, the Faraglione Colombaio and Faraglione Nerone, rising from the sea on the northern side of the island. It was established around 1400 BCE in a coastal area bordered by sea cliffs reaching a height of about 20 m and crowned by a Tyrrhenian marine terrace (Holloway and Lukesh, 1995, 2001; Foresta Martin and Frurlani, 2021), (Fig. 2).

The cliff is prone to continuous rockfalls and collapses, which likely had an impact on the village's life. Archaeologists have conducted several excavations in this area, revealing the remains of a settlement considered one of the most important and well-preserved towns from the Middle Bronze Age in the Mediterranean region (Mannino, 1970, 1979, 1982; Holloway and Lukesh, 1995, 2001; Spatafora, 2005; Spatafora et al., 2008; Counts and Tuck, 2009).

A massive fortified wall measuring about 250 m in length and 4 m in height was constructed to protect the village on the inland side. It was reinforced by thirteen or fourteen buttresses and encloses an area of

Fig. 4. The narrow main street (Street I) of "Faraglioni" village and the ruins of prehistoric huts.

Fig. 5. High-footed cups and other types of pottery recovered during archaeological excavations at the Middle Bronze Age Faraglioni Village. Carmelo Seminara Archaeological Museum of Ustica.

approximately 7000 square meters. Within this area, several huts, situated closely together along streets about 1 m wide, have been unearthed. The settlement displays an urban layout (Fig. 3) similar to that of the contemporary village of Thapsos, near Syracuse, Eastern Sicily. The excavated areas thus far reveal what appears to be the main street of the village, Street I (Fig. 4), running roughly from northwest to southeast, intersected by other narrow streets. Overlooking these streets are huts of circular or square shape, constructed with dry stone walls. Groups of adjacent huts shared courtyards, where containers for food and large "pithoi" or rainwater collection jars were placed (Holloway and Lukesh, 1995, 2001; Spatafora et al., 2008) (Fig. 4). The number of huts in the Village has been a subject of debate among different excavators over the past decades: Mannino (1982) suggested a few hundred, also considering an extension of the village in areas that later collapsed into the sea, while Holloway and Lukesh (1995) proposed only a few dozen.

Numerous well-preserved artifacts have been uncovered from within the huts, including a significant amount of ceramic containers for dining and food storage. Some of the vases show stylistic resemblances to contemporaneous ceramics from Milazzese Village (Panarea, Aeolian Island), while others bear the characteristics of the Thapsos Style. This style is marked by deep truncated cone bowls with high pedestal feet, likely used for consuming meals while seated on the ground (Fig. 5). The presence of five stone molds for casting bronze tools within the village suggests the activity of a workshop (Holloway and Lukesh, 1995, 2001; Spatafora et al., 2008).

3.2. An high standard of living

The diversity of furnishings and the organized living arrangements indicate that the Villaggio dei Faraglioni community engaged in fishing, agriculture, animal husbandry, and craftsmanship. Simultaneously, the logical urban layout and the abundance of furnishing within the huts attest to a well-structured social and economic organization, as well as a high quality of life for the inhabitants (Holloway and Lukesh, 1995, 2001; Spatafora et al., 2008).

Villaggio dei Faraglioni lay along Mediterranean trade routes, evident in its connection to the contemporary Sicilian culture of Thapsos through ceramics (Voza, 1972). Some shards with incised decoration in the Apennines style point to the island's involvement in Tyrrhenian trade with the Italian peninsula (Holloway and Lukesh, 1995, 2001; Spatafora et al., 2008). Additionally, a fragment of Mycenaean pottery and a few glass paste necklace beads testify to sporadic long-distance contacts with Bronze Age mainland Greece.

Excavations at the Villaggio dei Faraglioni also unearthed several

Fig. 6. Enclosing wall.

hundred obsidian fragments from Lipari and Pantelleria. This finding indicates the continued use of this volcanic glass during the Middle Bronze Age, in contrast to observations in other contemporary Sicilian villages where a drastic reduction in the use of these lithic tools is evident (Tykot and Martin, 2020, and references therein).

The existence of the Village seems to have come to an end around 1200 BCE when the inhabitants suddenly abandoned it, as deduced from their household belongings left in their usual positions within the dwellings.Two main hypotheses have been proposed to explain this departure: a natural disaster that pushed the population to seek safer ground or an onslaught of marauders from the sea. However, other plausible explanations include a prolonged drought that forced the inhabitants to leave or an epidemic that led to the population's demise (Foresta Martin and Frurlani, 2021). After this still unexplained event, Ustica remained uninhabited for about eight centuries, until the 4th-3rd century BCE, during the Hellenistic-Roman Age, when there is evidence of a resurgence of permanent settlements on the island (Spatafora et al., 2008).

3.3. The wall

The still standing wall of the Faraglioni village is the main part of a highly complex fortification system, both in its structural function and in its social, cultural, and military aspects. The fortification was influenced by the geomorphology of the site. Indeed the village was situated on a promontory jutting out into the sea, so that the coastal side (northwestern) was defended by the high and steep cliff, while the landside (southeastern) was protected by a mighty curved wall resembling a fishhook, designed to enclose the promontory of land facing the sea.

The enclosing wall (Fig. 6) survives for a length of about 250 m and has a thickness of approximately 2.5 m at the top. The original heights must have ranged between 4 and 5 m (Holloway and Lukesh, 1995;

Fig. 7. Left) Outer and right) inner structure of Tower No. 12.

Fig. 8. Left) example of an ERT acquisition in the northern sector of the survey area, right) operators while performing the GPR survey in the southern sector.

Spatafora, 2016). It was constructed using the "sack wall" technique, meaning that it consisted of two parallel walls made of large stone blocks, with the central space filled with smaller stones. The construction was carried out without the use of binders, with the dry stones arranged appropriately.

On the outside, the perimeter wall is marked by a sequence of 13 buttresses and/or towers, at almost regular intervals, spaced between 12 and 16 m apart (Fig. 3) (Spatafora, 2016).

The inner side of the wall features a long walkway that protrudes about 1.50 m from the inner face of the fortification. Between this

Fig. 9. Left panel) ERT profiles (solid yellow lines). Right panel b) GPR profiles (solid red lines) acquired during the geophysical survey. The red box in panel left, indicates the position of the subset area in which GPR profiles were performed. Both acquisition layouts are superimposed to a high-resolution orthographic picture of the investigated area (Russolillo et al., 2022). Some profiles from different investigation techniques overlap (ex. P4 with T2, P5 with T10 and P6 with T21). (For interpretation of the references to colour in this figure legend, the reader is referred to the web version of this article.)

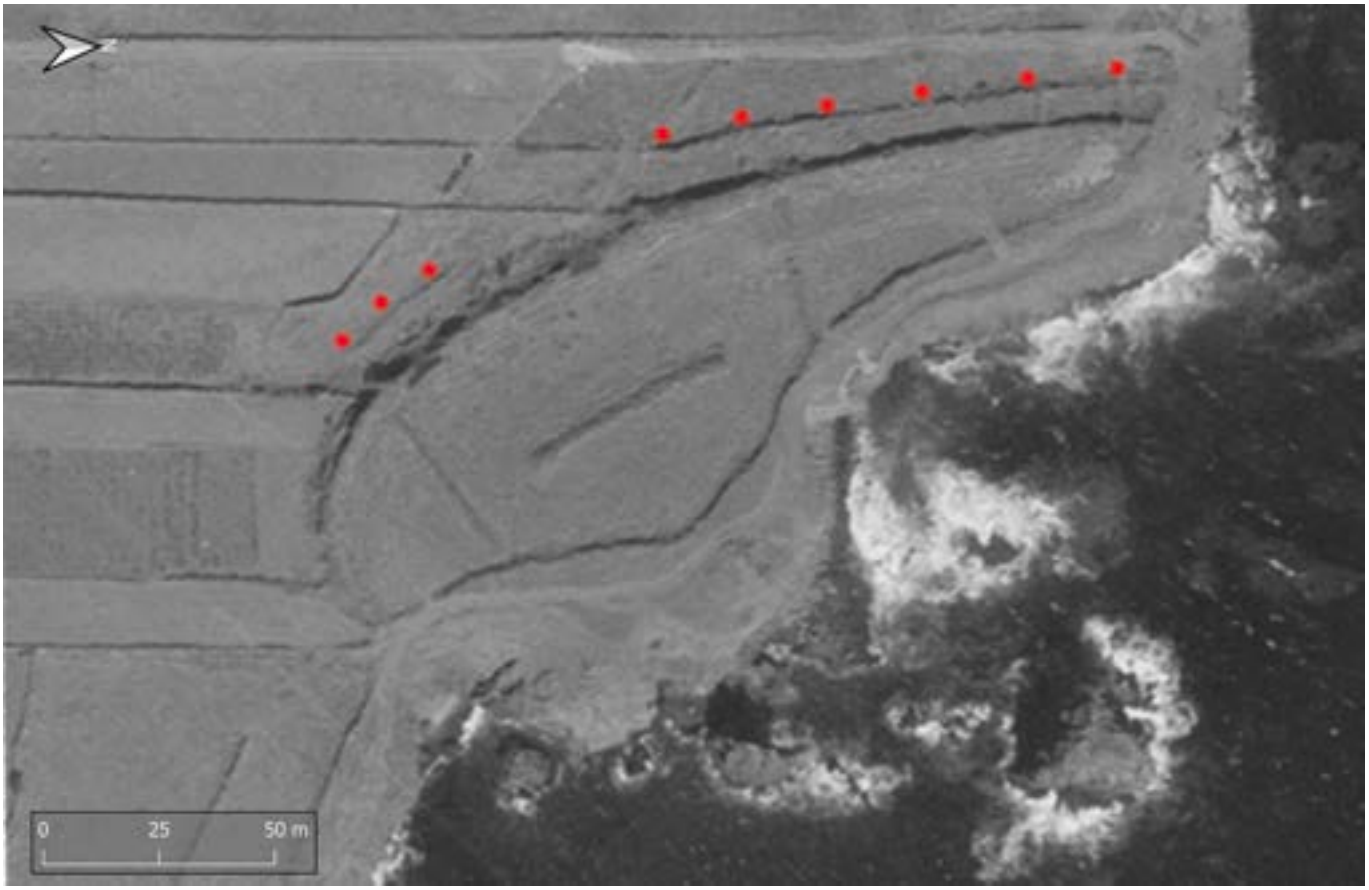

Fig. 10. Evidence of boulders alignment in front of the defensive wall on a 1968 aerial photo (SAS TD Palermo- IGM).

walkway and the village huts, there is a narrow path, about 1 to 1.50 m wide, which serves as a passageway between the houses and the enclosing wall. Of particular interest for our study is the complex Structure No. 12 (the second one from the north) (Fig. 7), consisting of a semicircular tower of approximately 3 m in diameter incorporated into another semicircular structure, both leaning against the perimeter wall. These two structures are in turn enclosed by a quadrangular forward extension that defines a corridor about 1.50 m wide (Spatafora, 2016). This structure was found to be connected to the outwork unveiled in the present study.

The construction of such a complex wall structure (perimeter walls, buttresses, towers, enclosures, moats) around a space served a dual purpose: defense and defining/limiting the area considered as belonging to the inhabiting human group. Its realization suggests a social structure (extended or smaller families, clans), wherein the communal construction of a defensive work also becomes an expression of belonging. Its construction, therefore, represented not only a defensive factor but also a unifying element for the community (Skeates, 2002; Parkinson and Duffy, 2007; Palio, 2020).

4. Methods

Geophysical prospecting was conducted on the eastern and southern sectors of the Villaggio dei Faraglioni site, involving both ERT and GPR acquisition techniques. To better emphasize the possible presence of electrical resistivity contrast associated with the buried wall structure, ERT profiles were performed orthogonally to the outcropping wall trace (where visible). Given the limited spaces, it was possible to run short ERT profiles, purposely centered to the hypothetical buried wall trace (Fig. 8, left). Consistent with the GPR survey, profiles and acquisition grids were concentrated in the northern sector, where logistics were favourable to dragging an antenna to the ground (Fig. 8, right).

The ERT and GPR prospections were preceded by the acquisitions of aerial images in different sunlight and seasonal environmental conditions, using Unmanned Aerial Vehicles (UAVs) equipped with multispectral sensors for imaging in visible light and infrared (Russolillo et al., 2022). The evolution of the landscape and archaeological ruins since the 1960s was also analyzed through the acquisition of historical aerial photographs available by the Istituto Geografico Militare (IGM) and Google Earth (Fig. 9, left and Fig. 10).

4.1. Electric resistivity tomography (ERT)

We deployed an array of 16 and 32 steel electrodes (1 m apart) to acquire 10 ERT short profiles (named from P1 to P10, Fig. 8), and a longer one (named P11) for a total of n. 11 ERT profiles, using a Syscal R2 (IRIS Instrument). The latter was facilitated by favourable logistics with no structural barriers to the east, which allowed us to extend the investigation eastward using a longer profile. With this configuration, we reached an average investigation depth of about 4 m below ground level (bgl) for ERT profiles P1 to P10 and of approximately 7 m for ERT P11. We injected a bi-polar square pulse of 250 ms generated by a 100 V energy source, using both dipole–dipole (DD) and Wenner-Schlumberger (WS) configurations, sensitive to horizontal and vertical changes in resistivity and thus suitable to accurately image shallow subsurface structures. Salt water was employed to enhance coupling between the electrodes and the ground, which returned an average measured resistance contact below 5 kΩm. We acquired a set of n. 84 and n. 49 measurement quadrupoles, respectively for DD and WS array of ERT P1 to P10 while n. 351 and n. 225 quadrupoles for DD and WS array of ERT P11. First electrodes were set to be in the opposite position of the main outcropping wall (i.e. west, south-west and south directions,

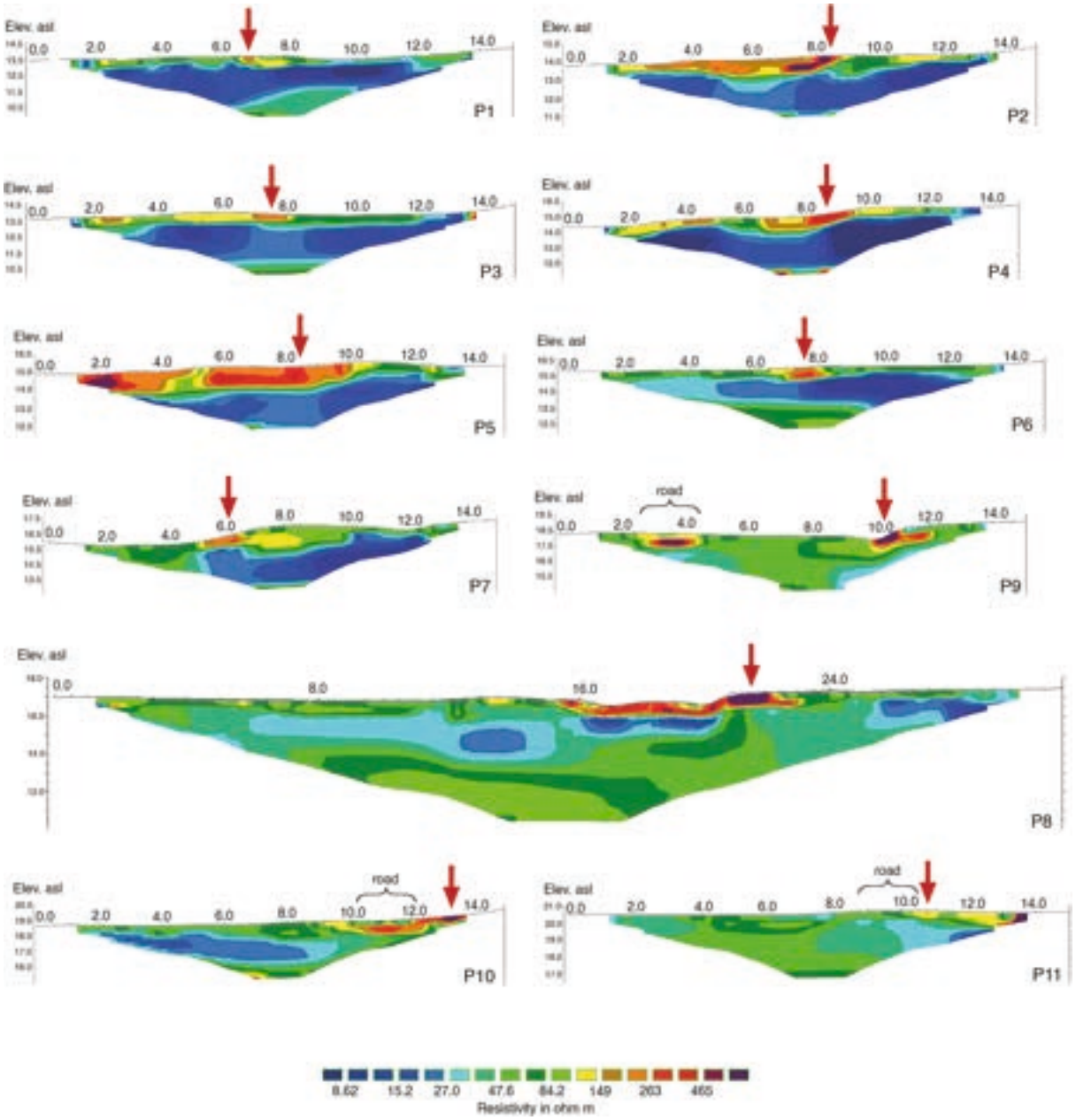

Fig. 11. ERT resistivity sections from P1 to P11; Absolute error (Abs. err) after six iterations are: P1, 2.3%; P2, 4.1%; P3, 2.9%; P4, 4.4%; P5, 4.7%; P6, 1.9%; P7, 4.1%; P8, 3.2%; P9, 4.3%; P10, 3.2% and P11, 4.0%. Red arrows indicate the position of the shallow high-resistive anomaly. (For interpretation of the references to colour in this figure legend, the reader is referred to the web version of this article.)

respectively), and the ERT profiles coordinates were measured using a differential GPS, to gather accurate topographic information for each electrode position.

The processing workflow consisted in filtering and despiking of clearly noisy data as derived from very low voltage and/or injected current in the ground. In general, data quality was found to be very high, and thus only few measurements were culled from each ERT dataset. Despiked and filtered raw apparent resistivity data represented the input to a 2-D regularized least squares inversion algorithm (Loke and Barker, 1995), using sharp constraints (L1-norm, robust inversion) to cope with the expected lateral resistivity contrast arising from the buried archaeological targets and the host soil. We parameterized the inversion using a starting model of 100 Ωm, which we assigned based on the evidence of volcanic deposits and outcropping bricks of volcanic origin with a reasonably high resistivity background.

We built a finite element (FE) 2-D mesh of rectangular blocks whose width is equal to half of the electrode spacing in the uppermost levels (0.5 m × 0.25 m). Model discretization linearly increases by 10% with each incremental depth interval. We jointly inverted DD and WS to gather a 2-D resistivity model that benefits from both vertical and horizontal resolution capabilities of the two adopted electrical array configurations. The quality of the recovered resistivity sections is then described by the absolute error after the last iteration, which is generally below 5% after 6 iterations for the entire set of elaborated tomographic models.

4.2. *Ground penetrating radar (GPR)*

GPR is a technique based on the principle of the propagation of EM electromagnetic waves in materials and on their reflection at the discontinuity surfaces due to variations in the dielectric permittivity of the investigated materials. The operating principle of the ground

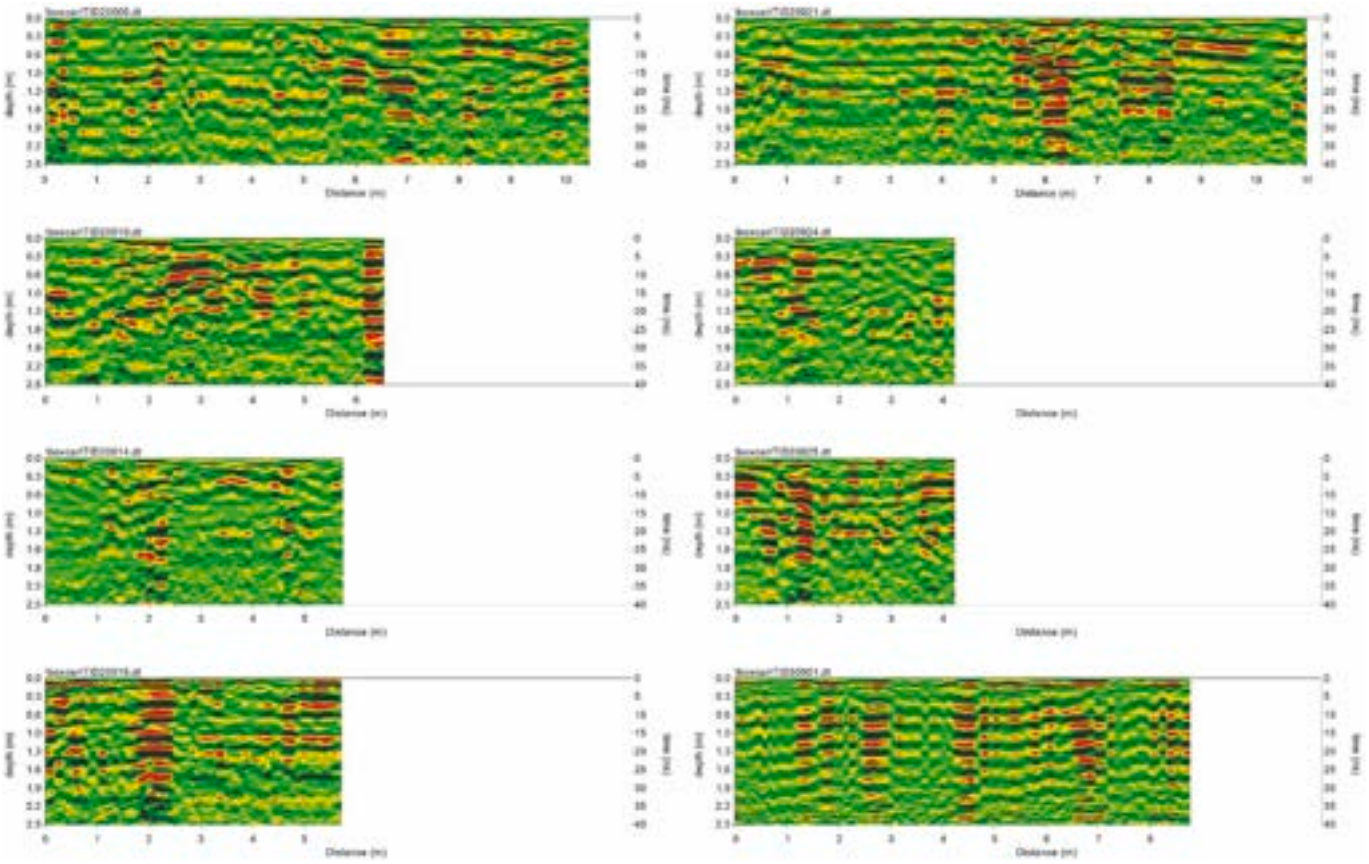

Fig. 12. Most representative b-scan profiles.

penetrating radar can be summarised as follows: an antenna is dragged over the surface producing EM waves that propagate through the subsoil; energy is thus reflected at the interfaces between units or bodies characterised by different dielectric properties so that the reflected signal is captured by an integrated receiving antenna, placed on the surface. The depth of investigation and the resolution capability of a GPR system is a complex function of three main factors: i) the central frequency of the antenna, ii) the soil conditions and iii) the physical and geometrical characteristics of the target (such as size, shape, and composition). Generally, higher central frequency antennas have better resolution but lower depth penetration, while lower central frequency antennas have lower resolution but deeper penetration. Moist soil can reduce the depth of penetration due to the high attenuation of the electromagnetic waves, while dry soil can allow deeper penetration. For GPR data, we used an IDS HiMod equipped with 400\900 MHz central-frequency antenna to acquire a set of parallel profiles approximately oriented W-E, with different lengths, within a survey grid of 16 × 30 m, overlapping three ERT profiles. A total of 27 b-scans (two-dimensional reflection profiles) were collected: we recorded the data in one direction, as a gridded mesh was not feasible, due to the presence of obstacles on the site. As for ERT profiles, we collected the start and end points of GPR scans with a GNSS receiver with real-time kinematic corrections (RTK).

The instrumental parameters, set before acquisition, include a time window of 80 ns and a scan resolution of 512 samples/scan; after detection of time-0 these values have been adjusted to a time window of 75 ns and 482 samples/scan.

GPR data, available for both 400 MHz and 900 MHz central-frequency range, were processed with the software GPR-Slice (powered by Screening Eagle Technology). The processing steps aimed at filtering the raw signals, correcting noise effects, and yielding clean and easily interpretable b-scan sections and time-slices. To achieve this, we implemented the following filtering algorithms:

- Background noise subtraction, to subtract constant noise due to instrumental interference from scans.
- Bandpass filter, to remove high and low-frequency noise. The thresholds were set as 200 MHz (low-pass) and 725 MHz (high-pass), approximately 1.5 times lower and higher than the central frequency of the antenna.
- Manual gain, to enhance the features after the noise reduction caused by background removal. The gain curve was set to include both a linear and an exponential component.
- Boxcar filtering, to smooth high-frequency random noise in GPR scans. In this instance, the dimensions of the boxcar window are 1 pixel by 1 pixel.
- Hyperbola migration, to assess the velocity model of the terrain and better estimate depths. Through the empirical method of hyperbola fitting, the velocity was estimated as 0.113 m/ns (corresponding to a dielectric constant of 7.4).
- Hilbert transformation, to convolute data into positive-amplitude domain and perform the interpolations which yield the time-slices.

As part of the filtering procedure, we tried the implementation of spectral whitening to achieve spectral equalisation of the signal and to recover high-frequency detail which may have been lost in bandpass filtering (Leckebusch, 2005). However, this proved ineffective, as the b-scans which went through this algorithm ended up losing most of their informative content. Therefore, we concluded that in this context, which is quite undisturbed by utilities and offers most of its content within the uppermost 2 m of depth, spectral whitening is not only unnecessary, but rather counterproductive.

We found that although 900 MHz scans allow for a cleaner overall image, the increase in frequency brings a significant drop in depth of

Fig. 13. Red lines highlight on the left the northern section of the wall; on the right the semi-buried boulders that constitute remnants of the Faraglioni outwork system. (For interpretation of the references to colour in this figure legend, the reader is referred to the web version of this article.)

investigation (signal/noise ratio drops at 50 cm depth), so we preferred the 400 MHz profiles for analysis and detection of anomalies.

In performing time-slice analysis, we employed a slicing/gridding approach to obtain 50 5-cm thick slices, to which we then applied a 3 × 3 low pass filter in order to smoothen the images and reduce the impact of high-frequency noise caused by the inverse distance weighted (IDW) interpolation. From these slices, we then produced a 3D volume, on which we performed an overlay analysis between an interval of depth between about 0.6 and 0.8 m. This analysis allowed us to enhance features we believe are of great interest, and correlate very well with ERT results.

5. Geophysical results

Results from the inversion of the entire set of acquired ERT profiles are shown in Fig. 11. Overall, the recovered ERT sections highlight a three-layered subsurface resistivity distribution with an uppermost moderately resistive cover, of variable thicknesses, on top of a low-resistive layer with sub-horizontal geometry. At depth, the models hint to an increase in resistivity of the subsoil.

More in detail, the uppermost moderately resistive layer shows average resistivity values of approximately 80–100 Ωm and a thickness of about 0.5–1 m. This is quite visible for ERTs P1 to ERT P7 resistivity sections except for ERT P5 where we observe a slightly thicker uppermost layer, which gets thinner toward East. For ERTs P8 to P11, this shallower layer is barely visible and its resistivity slightly decreases. Within this layer, we observe a high-resistive anomaly ($\rho > 200$ Ωm), about 2 m wide and approximately 0.5 m deep, that occurs in all ERT profiles. This anomaly is almost centered in ERTs profile P1 to P7 while it appears shifted eastward for ERT profiles located further south (ERTs P8 to P11, Fig. 11). It shows a rectangular-like shape that in some sections seems to be disarticulated into distinct anomalies of irregular shapes with associated high resistivity (i.e. P2 and P8). This anomaly does not show a uniform resistivity signature in all ERT profiles. In some cases, it exhibits a weaker resistivity contrast compared to others where it is more pronounced. For instance, in profile P5, this anomaly is difficult to interpret as it is blurred within a high resistivity layer, while in profile P11, it appears to be less resistive ($\rho \sim 140$ Ωm), with values comparable to those detected in profile P1. It is worth to note that for the southernmost profiles, particularly for P10 and P11, this anomaly falls either directly on (in the case of P10) or in close proximity to (in the case of P11) a recently constructed trail, which makes its attribution more difficult.

Below the resistive cover, a low-resistivity layer ($\rho < 30$ Ωm) occurs with variable thicknesses ranging between 2 m up to a maximum of 3 m down to the bottom of the ERT sections. Where the thickness is reduced to about 2 m, an additional layer comes up in which the resistivity seems to slightly increase (i.e. P1, P3, P6 and P8). On the other hand, in ERT P9 and P11 this low-resistive unit appears to be confined to the edges of the sections, which instead consist of a moderately resistive background down to the bottom of the models ($\rho \sim 60$ Ωm).

Among the results collected through GPR investigation, we selected a set of n.8 GPR b-scans which better highlight the representative reflection patterns, in which high-energy anomalies are especially notable (Fig. 12). Below a shallow layer with low energetic response, GPR b-scans display a concentration of dielectric contrast, a clear indicator of a change in material velocity and composition. Although some of the scans appear characterised by a severely scattered behaviour (most notably in profiles T5 and T14), the reflections describe reflectors with approximately rectangular shape, with a width of about 1.5 m (which would be comparable with that of the inferred stone boulders) and persist until about 2 m bgl, from which we observe a notable loss in signal resolution, possibly due to the presence of a conductive layer in which electromagnetic signal rapidly attenuates. Such a shift in subsurface properties is observed in ERT profiles too, where a low-resistivity interface can be recognised about 2 m deep. We thus consider this depth as the maximum extent of investigation for GPR methodology.

Some profiles exhibit multiple distinct anomalies, yet we assume that the inferred reflector is linear and relatively continuous. To confirm which reflections can be attributed to a single, continuous structure, we conducted a 3D visualisation of the b-scans. This visualisation reveals that these anomalies form a sequence of GPR reflections aligned and parallel to the outcropping wall trace encircling the village (see Fig. 16).

6. Discussion

6.1. Resistivity and lithology

According to our observations carried out on the outcropping lithologies, the subsurface distribution of geophysical anomalies can be interpreted as follows.

The uppermost, moderately resistive layer ($\rho \sim 80$–100 Ωm) can be easily correlated to the present walking ground, which represents the subaerial evolution of an erosional surface of marine origin cut in a lava bedrock, and its humified, continental, sedimentary covering (de Vita, 1993; de Vita et al., 1998). In its uppermost 0.5–1 m this covering is composed of a hardly compacted and dry, heterometric and heterogeneous, detrital deposit, mainly made of gravel and pebble clasts in a clayey-sand matrix. The thickness of this layer increases toward south and grades downward in a more soft, loose and deeply humidified and clay-rich deposit with an increasing degree of humidity. This explains

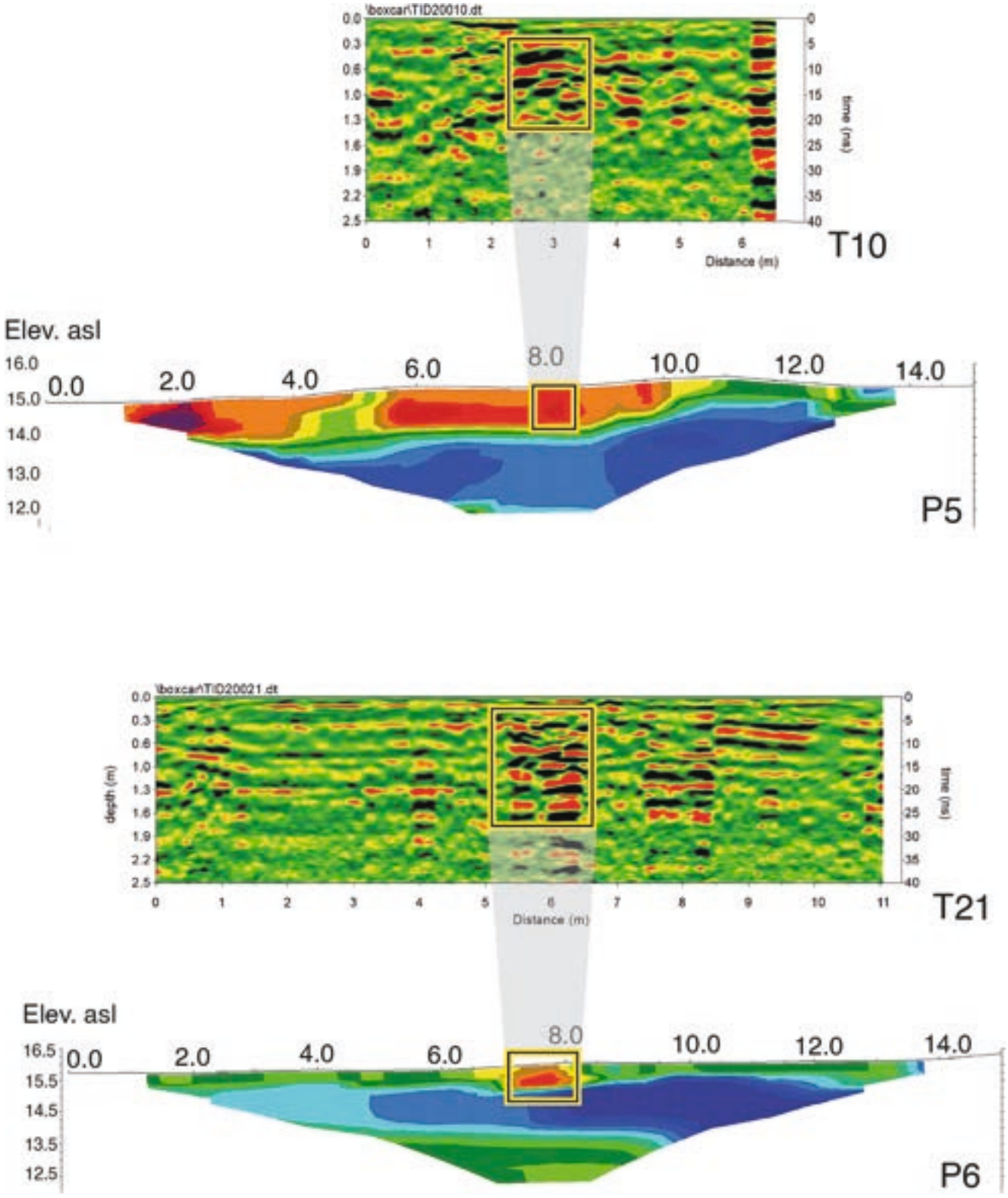

Fig. 14. ERT and GPR output model comparison over overlapping profile (see Fig. 9, right for profile location).

the more or less continuous and less resistive horizon ($\rho < 30$ Ωm), visible in ERT profiles P1-P7 (Fig. 10), with a thickness ranging between 2 and 3 m.

The rectangular-shaped high-resistivity anomaly ($\rho > 250$ Ωm) included in this layer corresponds to stacks of large lava boulders, partially buried and locally exposed, more or less in the middle part of the ERT profiles. The anomaly extends downward to a depth of about 0.5 m and is interpreted as due to the higher resistivity of the boulders and to the presence of air into the empty space among them. The same occurs toward the southern end of P4 and P5 (Fig. 10), where similar large blocks, likely fallen (or anthropically removed and displaced) from the stacks, are buried at a shallow depth.

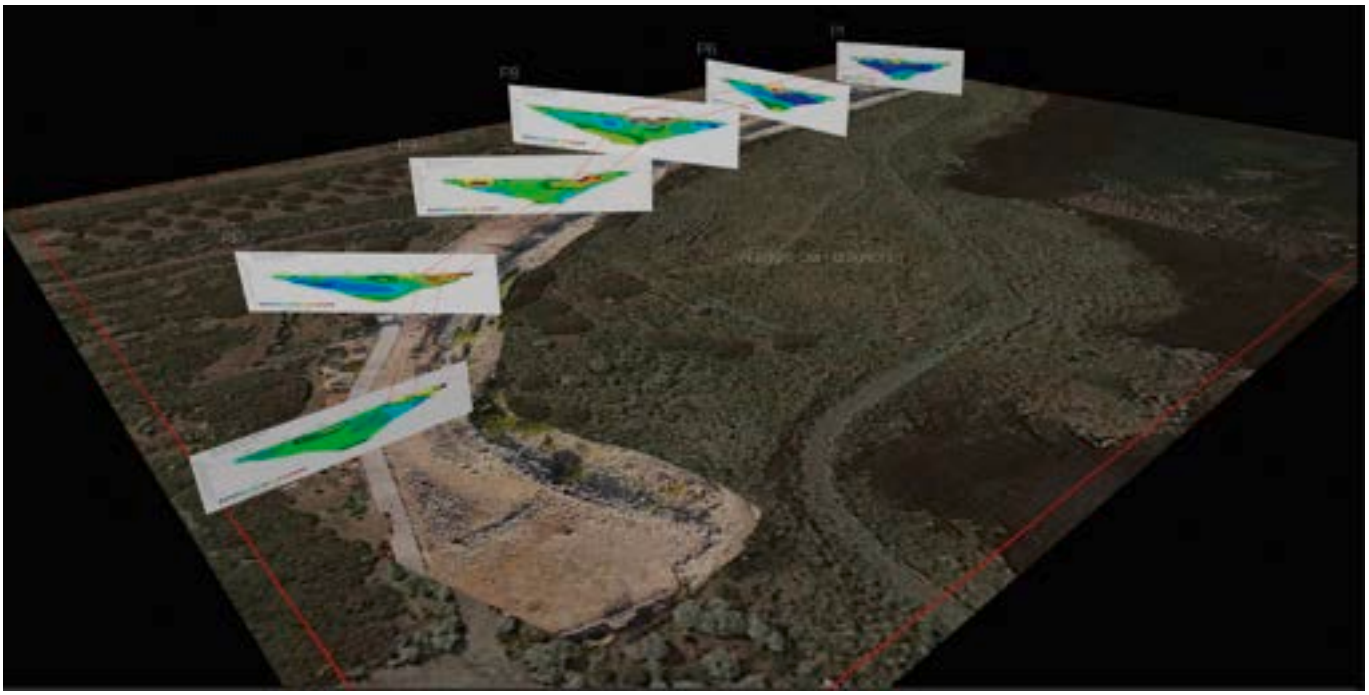

Fig. 15. 3D composite of the ERT profiles in which the resistivity anomaly associated to the inner wall is interpolated through highlighting the potential traces of the buried outer wall of Villaggio dei Faraglioni.

A downward increase in resistivity, evidenced below the intermediate low-resistivity layer, is recorded in almost all profiles (i.e. P1, P3, P6 and P8; $\rho \sim 60$ Ωm; Fig. 11) and particularly in the deepest part of P4 ($\rho > 250$ Ωm; Fig. 11). In this case it has been interpreted as the contact with the underlying weathered lava bedrock.

6.2. The semi-buried wall

In the preliminary phase of this research, we focused our observations on the outer part (southward) of the Faraglioni fortification system (Russolillo et al., 2022). Data gathered on the field coupled with historical aerial imagery highlighted the remnants of a linear structure made of semi-buried boulders. It develops at a distance of about 6–7 m eastward from the wall and follows discontinuously its arched course, emerging clearly on the surface only in the northernmost sector of the fortification (Fig. 13).

At first glance, these emergencies could be mistaken for boulders rolled down by the collapse of the defensive wall, and then naturally covered by farmland. However, the emerging segments of the boulders are aligned with the wall, and therefore to further investigate if this alignment may correspond to another wall structure at depth we carried out ERT and GPR geophysical prospection. The employed techniques highlighted a pattern of geophysical anomalies, which can be recognised in both ERT and GPR sections. Firstly, we compare the results obtained from the ERT and GPR survey over two overlapping profile (Fig. 14). ERT anomalies are characterised by a high-resistive rectangular-like shaped (roughly 2 m wide and 1 m thick) anomaly with resistivity ranging from 150 up to about 500 Ωm. Radar data show clear high-energy reflections that stand out from the background. This dielectric behaviour allowed us to estimate the geometrical properties of the target with a higher degree of confidence: the persistence in depth of the anomaly ranges from 0.5 m to 1.5 m starting at very shallow levels (about 0.3 m), while its thickness is almost always about 1 m. Considering the distribution of the ERT anomalies along the inner wall, we attempted to reconstruct a possible path of the investigated target through a rough interpolation between profiles. By doing this, we observed that there is an along-path alignment lying at a distance of approximately 6 m from the outcropping wall in the northernmost sector (Fig. 15); this distance progressively decreases.

toward southwest, getting closer to the inner defensive line. Noteworthy, the external face of a large and articulated tower standing in the northern section of the wall (Tower 12) (Fig. 7) seems to be connected with this outwork. However, in the ERT profiles P10 and P11, the interpretation of the resistive anomaly associated with the presence of the buried wall is more uncertain. This is due to the presence of a recent road that may have altered the structure of the wall itself thus masking the expected resistivity response as we observed in the other ERT profiles. However, it is equally true that the road itself does not show a clear anomaly in the resistivity sections. Indeed, the road is intercepted in the initial portion of profile P9, between 2.5 m and 4.5 m distances along the profile, and it coincides with a high resistivity anomaly ($\rho \sim 400$ Ωm), about 1 m deep, as evidenced in the resistivity section (Fig. 11). In profile P10, the road is confined between the distances of 8.5 m and 10.5 m of the resistivity section in which we observe a slightly resistive anomaly ($\rho \sim 150$ Ωm), about 1 m wide and 0.3 m thick in a barycentric position respect to the roadside. Conversely, in ERT P11, although the profile intersects with the road roughly at the same location as for P10, we didn't observe a clear resistivity anomaly which in turn appears with a lower resistivity response ($\rho \sim 150$ Ωm, Fig. 11) located at the edge of the road. While we would expect the presence of the road base and pavement to generate a high resistivity response in the ERT sections, on the other hand, we expect this target to be very shallow (<0.3 m) and likely not clearly resolvable with the adopted electrode spacing. We thus believe that the recent road was actually built on or very close to the buried wall structure, and we infer that the presence of the road and the underlying and\or bordering wall structure both contribute to the observed resistivity anomaly of the ERT sections acquired in this portion of the survey area. Like we did for ERT data, we positioned our dataset in 3D space to observe the distribution of dielectric variations. The results, shown in Fig. 16, reveal a compelling correlation with the findings from the resistivity analysis. The implementation of time-slice analysis allowed us to produce a series of horizontal depth maps: the overlay operation we conducted between the levels of −0.6 and − 0.8 m below ground level (b.g.l.) highlighted the expected alignment of dielectric

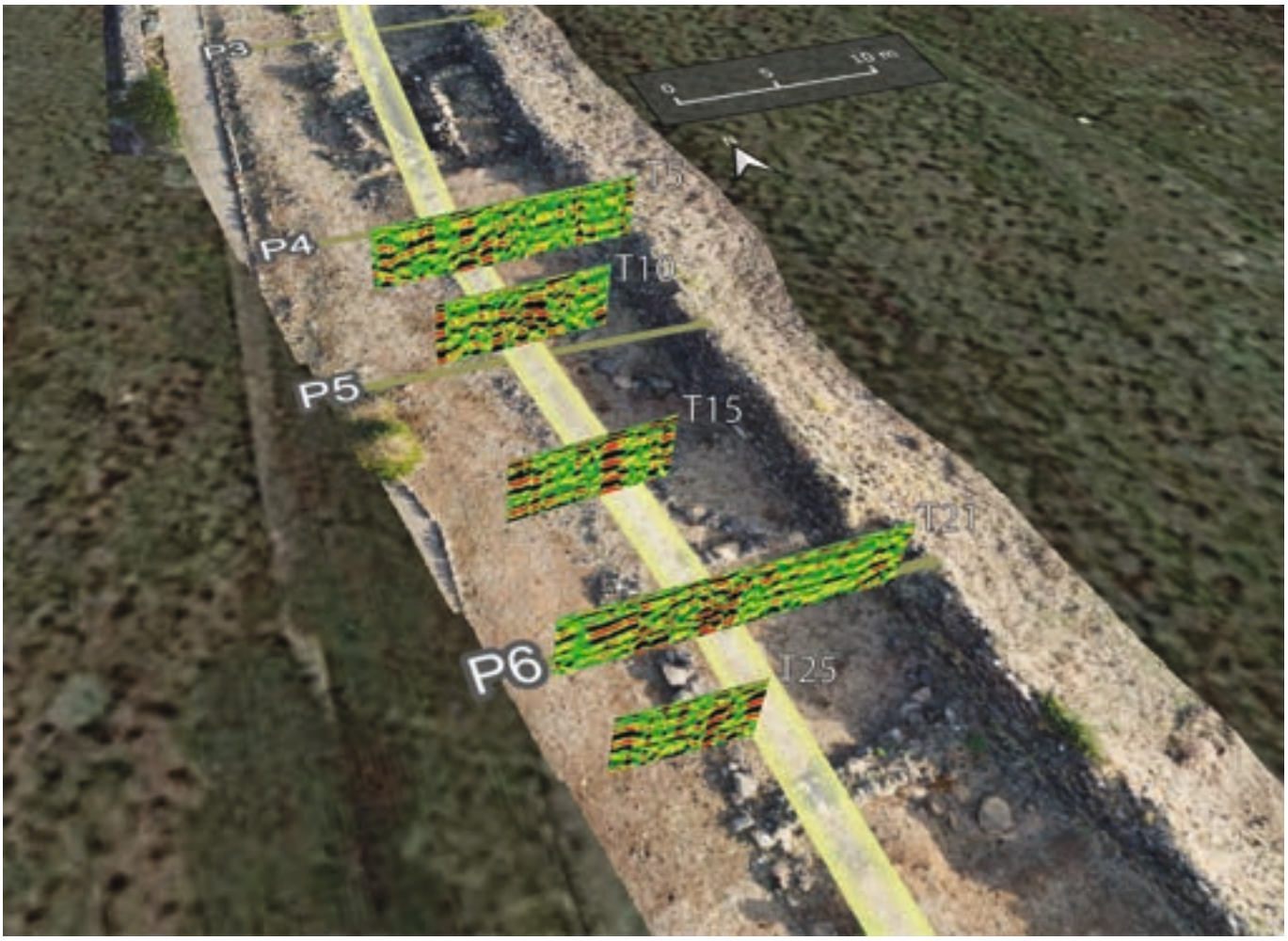

Fig. 16. 3D view of GPR b-scan. The yellow path represents the inferred wall trace as interpreted from the ERT results. (For interpretation of the references to colour in this figure legend, the reader is referred to the web version of this article.)

reflections, which falls exactly on the trace of the interpolated ERT anomalies (Fig. 17), although the presence of the reflections is quite discontinuous and it often depicts irregular and non-bounded geometries; we infer that this behaviour may be due to the state of conservation of the wall itself, as a poor state of conservation of the buried targets or deeply altered artifacts could, in some instances, cause a depolarisation of materials and EM signal scattering (Conyers, 2015). This may be confirmed by ERT readings, which show anomalies ranging in a wide spectrum of resistivity values (i.e. ERT profiles P1, P5 and P11). The defensive system of the Faraglioni Village seems to follow the typology of the Roca Middle Bronze Age settlement, which is considered as one of the most important archaeological sites for the study of Italian and Mediterranean proto-history. In the 2nd millennium BCE, this site was protected by imposing fortifications characterised by two parallel walls separated by a large corridor, a main gate, and some posters (Scarano, 2012). In the case of Ustica, however, the gates have not yet been located with certainty. Further investigations, accompanied by some excavation tests in the area, will be necessary to better understand the stratigraphy and morphology of this new evidence as well as the timing of this construction with respect to the prehistoric occupation of the area.

7. Conclusions

We remark that the geophysical prospecting campaign led out in this study is the former carried out so far at the Faraglioni Village of Ustica. In the light of the new evidence, it could be assumed that the defensive system of the Faraglioni Middle Bronze Age village at Ustica consisted of two main elements: a large peripheral outwork, and an internal wall reinforced by buttresses, both having an arched design and mutually distant 6–7 m; their construction was aimed at isolating the marine terrace and the village from the Tramontana plain. While the internal wall is today largely intact, and still standing up with a maximum height of 4 m (despite many of its top parts and its buttresses having been used as a stone quarry after the abandonment of the village), the outwork has been completely dismantled and only a few basal boulders emerge from the ground in some sections.

The application of geophysical prospecting techniques described in this paper has proven to be highly satisfactory in terms of both the obtained results and the multidisciplinary interpretation of the data. However, while the information regarding the buried structures is well established, the strictly archaeological aspects have not been thoroughly explored in terms of conclusive interpretations regarding the temporal, constructional, and cultural relationships among the observed structures. Nonetheless, the usefulness of the applied geophysical prospecting is prominently highlighted in this paper, particularly in its ability to investigate sites of archaeological and historical significance in a non-invasive manner. By doing so, it avoids the need for costly excavation operations in the immediate future, instead focusing on subsequent targeted investigations. This approach undoubtedly brings about economic advantages and optimizes both field work and financial resources. In this sense, territorial managers and superintendents

Fig. 17. Time-slice analysis between 0.6 and 0.8 m that highlight a clear alignment of electromagnetic reflection, which also aligns with the inferred wall trace interpreted from ERT anomalies.

appointed for the protection of the cultural heritage can derive the maximum benefit from this kind of investigation and configure themself as its main stakeholder, beyond the purely scientific contribution to the study and knowledge of both the territory itself and the history of human settlements.

Lastly, we have plans to conduct additional non-invasive investigations in the near future, which will hopefully be followed by excavation tests. These tests are necessary to address the remaining unanswered questions concerning the evolution and demise of this valuable Middle Bronze Age settlement located in the heart of the Mediterranean Sea.

CRediT authorship contribution statement

Anna Russolillo: Writing – review & editing, Writing – original draft, Validation, Supervision, Project administration, Conceptualization. **Franco Foresta Martin:** Writing – original draft, Investigation, Formal analysis. **Antonio Merico:** Writing – original draft, Software, Methodology, Formal analysis, Data curation. **Vincenzo Sapia:** Writing – review & editing, Writing – original draft, Methodology, Investigation, Formal analysis, Data curation. **Pierfrancesco Talamo:** Writing – review & editing, Validation, Conceptualization. **Valerio Materni:** Methodology, Investigation, Data curation. **Marta Pischiutta:** Writing – review & editing, Methodology, Investigation. **Sandro de Vita:** Writing – original draft, Visualization, Validation, Supervision, Formal analysis. **Stefano Furlani:** Writing – review & editing, Validation, Project administration. **Domenico Targia:** Validation, Supervision, Project administration. **Mauro A. Di Vito:** Validation, Supervision, Project administration, Funding acquisition.

Declaration of Competing Interest

The authors declare that they have no known competing financial interests or personal relationships that could have appeared to influence

the work reported in this paper.

Data availability

Data will be made available on request.

Acknowledgments

This investigation was conducted thanks to the financial support of the project Brains2Islands, “Indagine Multidisciplinare nei Contesti Insulari Basso Tirrenici”, funded by FONDAZIONE CON IL SUD, project number 2015-0296. We V. Ambrosanio, 2022. We thank the Parco Archeologico di Himera Solunto e Iato that encouraged this study. We also would like to thank the Comune di Ustica, AMP Ustica and Forestale Ustica institutions.

References

Akca, İ., Balkaya, Ç., Pülz, A., Alanyalı, H.S., Kaya, M.A., 2019. Integrated geophysical investigations to reconstruct the archaeological features in the episcopal district of Side (Antalya, Southern Turkey). J. Appl. Geophys. 163, 22–30.

Balkaya, Ç., Ekinci, Y.L., Çakmak, O., Blömer, M., Arnkens, J., Kaya, M.A., 2021. A challenging archaeo-geophysical exploration through GPR and ERT surveys on the Keber Tepe, City Hill of Doliche, Commagene (Gaziantep, SE Turkey). J. Appl. Geophys. 186, 104272.

Barberi, F., Innocenti, F., 1980. Volcanisme Neogéne et Quaternaire. Guide a l’excursion 122-A. Soc. It. Miner. Petrol. 99–104.

Barberi, F., Borsi, S., Ferrara, G., Innocenti, F., 1969. Strontium isotopic composition of some recent basic volcanites of the Southern Tyrrhenian Sea and Sicily Channel. Contrib. Mineral. Petrol. 23, 157–172. https://doi.org/10.1007/BF00375177.

Cinque, A., Civetta, L., Orsi, G., Peccerillo, A., 1988. Geology and geochemistry of the island of Ustica (Southern Tyrrhenian Sea). Boll. Soc. Ital. Miner. Petrol 43, 987–1002.

Conyers, L.B., 2015. Analysis and interpretation of GPR datasets for integrated archaeological mapping. Near Surf. Geophys. 13, 645–651. https://doi.org/10.3997/1873-0604.2015018.

Corradini, E., Wilken, D., Zanon, M., Groß, D., Lübke, H., Panning, D., Dörfler, W., Rusch, K., Mecking, R., Erkul, E., Pickartz, N., Feeser, I., Rabbel, W., 2020. Reconstructing the palaeoenvironment at the early Mesolithic site of Lake Duvensee: Ground-penetrating radar and geoarchaeology for 3D facies mapping. The Holocene 30 (6), 820–833. https://doi.org/10.1177/0959683620902234.

Corradini, E., Groß, D., Wunderlich, T., Lübke, H., Wilken, D., Erkul, E., Schmölcke, U., Rabbel, W., 2022. Finding Mesolithic Sites: a Multichannel Ground-Penetrating Radar (GPR) investigation at the Ancient Lake Duvensee. Remote Sens. 14, 781. https://doi.org/10.3390/rs14030781.

Counts, D.B., Tuck, A.S., 2009. Discovery and Dis course: Archaeology and Interpretation. In: Koine: Mediterranean Studies in Honor of R. Ross Holloway, Oxbow Books, Oxford.

de Vita, S., 1993. Assetto geologico-strutturale ed evoluzione vulcanologica dell’isola di Ustica (Stratigrafia, tettonica e meccanismi eruttivi). Tesi di dottorato, Napoli, p. 162.

de Vita, S., Foresta Martin, F., 2017. The palaeogeographic setting and the local environmental impact of the 130 ka Falconiera tuff-cone eruption (Ustica island, Italy). Ann. Geophys. 60 (2), S0224. https://doi.org/10.4401/ag-7113.

de Vita, S., Orsi, G., 1994. I terrazzi marini dell’isola di Ustica (mar Tirreno meridionale – Italia). Mem. Descr. Carta Geol. It. 52, 405–406.

de Vita, S., Guzzetta, G., Orsi, G., 1995. Deformational features of the Ustica volcanic area in the Southern Tyrrhenian Sea (Italy), 7, pp. 623–629. https://doi.org/10.1111/j.1365-3121.1995.tb00711.x.

de Vita, S., Laurenzi, M.A., Orsi, G., Voltaggio, M., 1998. Application of 40Ar/39Ar and 230Th dating methods to the chronostratigraphy of Quaternary basaltic volcanic areas: the Ustica island case history. Quat. Int. 47 (48), 117–127. https://doi.org/10.1016/S1040-6182(97)00077-3.

Di Mauro, M., Alfonsi, L., Sapia, V., Urbini, S., 2014. A neighborhood revealed by geophysical prospection: An example of urbanization at the Phoenician–Punic settlement of Mozia (Western Sicily, Italy). J. Appl. Geophys. 104, 114–120. https://doi.org/10.1016/j.jappgeo.2014.02.021.

Epimakhov, A.V., Berseneva, N.A., Fedorova, N.V., Noskevich, V.V., 2016. Geophysics and Archaeology of Bronze Age Settlements-a Case Study from Kamennyi Ambar Fortified Settlement (South Urals). Near Surface Geoscience 2016-22nd European meeting of Environmental and Engineering Geophysics (Vol. 2016, no. 1, pp. cp-495). European Association of Geoscientists & Engineers. https://doi.org/10.3997/2214-4609.201602029.

Foresta Martin, F., Frurlani, S., 2021. Geomorphology and prehistoric settlements on a Volcanic Island: the Case of Ustica (Palermo, Italy). Ann. Geophys. 64 https://doi.org/10.4401/ag-8703.

Holloway, R.R., Lukesh, S.S., 1995. Ustica I: Excavations of 1990 and 1991, Providence, Rhoe island Brown University, Louvain- La – Neuve. Belgium Universitè de Louvain 69–75.

Holloway, R.R., Lukesh, S.S., 2001. Ustica II: Excavations of 1994 and 1999. Rhoe island Brown University, Providence, pp. 3–21.

Leckebusch, J., 2005. Use of antenna arrays for GPR surveying in archaeology. Near Surf. Geophys. 3 (2), 111–115.

Loke, M.H., Barker, R.D., 1995. Least-square inversion of apparent resistivity pseudosections. Geophysics 60, 1682–1690. https://doi.org/10.1190/1.1443900.

Mannino, G., 1970. Ustica. Sicilia Archeologica 11, 37–41.

Mannino, G., 1979. Ustica: risultati di esplorazioni archeologiche. Sicilia Archeologica Tapani 12 (41), 7–40.

Mannino, G., 1982. Il villaggio dei Faraglioni di Ustica. Notizie preliminari. Studi in onore di Ferrante Rittatore Vonwiller 1 (1982), 280–297.

Mannino, G., 1991. Ustica: Nuove e più antiche testimonianze archeologiche. Sicilia Archeologica 24 (75), 65–85.

Mannino, G., 1997. Ustica (Palermo).

Mannino, G., 1998. Il neolitico nel palermitano e la nuova scoperta nell’isola di Ustica. Quaderni del Museo Archeologico Regionale “Antonio Salinas” 4, 56–57.

Mannino, G., 2015. La scoperta del Neolitico a Ustica. Lettera del Centro Studi e Documentazione Isola di Ustica 48-49, 30–35.

Mannino, G., Ailara, V., 2016. Carta Archeologica dell’isola di Ustica. Edizioni del Centro Studi e Documentazione Isola di Ustica, Ustica (Palermo).

Milo, P., Vágner, M., Tencer, T., Murín, I., 2022. Application of Geophysical Methods in Archaeological survey of early medieval Fortifications. Remote Sens. 14 (10), 2471. https://doi.org/10.3390/rs14102471.

Murín, I., Neumann, M., Brady, C., Bátora, J., Čapo, M., Drozd, D., 2022. Application of magnetometry, georadar (GPR) and geoelectrical methods in archaeo-geophysical investigation of a Napoleonic battlefield with fortification at Pressburg (Bratislava, Slovakia). J. Appl. Geophys. 196, 104493 https://doi.org/10.1016/j.jappgeo.2021.104493.

Neubauer, W., Eder-Hinterleitner, A., Seren, S., Melichar, P., 2002. Georadar in the Roman civil town Carnuntum, Austria: an approach for archaeological interpretation of GPR data. Archaeol. Prospect. 9 (3), 135–156. https://doi.org/10.1002/arp.183.

Orlando, L., Michetti, L.M., Belelli Marchesini, B., Papeschi, P., Giannino, F., 2019. Dense georadar survey for a large-scale reconstruction of the archaeological site of Pyrgi (Santa Severa, Rome). Archaeol. Prospect. 26 (4), 369–377. https://doi.org/10.1002/arp.1750.

Palio, O., 2020. Strutture difensive della Sicilia preistorica, tra Neolitico e Bronzo Antico. In: Calio, M.L., et al. (Eds.), Fortificazioni e società nel Mediterraneo occidentale. Atti del convegno di Archeologia organizzato dall’università di Catania, dal Politecnico di Bari e dalla University of Manchester. Catania-Siracusa 14–16 febbraio 2019. Edizioni Quasar, Roma, pp. 15–24.

Parkinson, W.A., Duffy, P.R., 2007. Fortifications and enclosures in European prehistory: a cross-cultural perspective. J. Archaeol. Res. 15, 97–141. https://doi.org/10.1007/s10814-007-9010-2.

Porcelli, F., Sambuelli, L., Comina, C., Spanò, A., Lingua, A., Calantropio, A., Catanzariti, G., Chiabrando, F., Fischanger, F., Maschio, P., Ellaithy, A., Airoldi, G., De Ruvo, V., 2020. Integrated geophysics and geomatics surveys in the Valley of the Kings. Sensors. 20 (6), 1552. https://doi.org/10.3390/s20061552.

Romano, R., Sturiale, C., 1971. Carta geologica dell’Isola di Ustica: R. Romano e C. Sturiale. Istituto internazionale di ricerche vulcanologiche. Istituto internazionale di vulcanologia (Catania, Italy).

Russolillo, A., Foresta Martin, F., Furlani, S., Talamo, P., Vinci, G., Zangara, S., 2022. The fortification system of the prehistoric Villaggio Dei Faraglioni on the Ustica island (Sicily): Some new data. In: Convegno Internazionale di Archeologia Aerea - Lecce.

Sapia, V., Materni, V., Florindo, F., Marchetti, M., Gasparini, A., Voltattorni, N., Civico, R., Giannattasio, F., Miconi, L., Marabottini, M.F., Urbini, S., 2021. Multi-parametric imaging of Etruscan chamber tombs: Grotte Di Castro Case Study (Italy). Appl. Sci. 11 (17), 7875. https://doi.org/10.3390/app11177875.

Scarano, T., 2012. Roca I. Le fortificazioni della media età del bronzo, Claudio Gerenzi Editore, pp. 63–93. http://www.jstor.org/stable/24308743.

Skeates, R., 2002. The social dynamics of enclosures in the Neolithic Tavoliere, South-East Italy. J. Mediterr. Archaeol. 13, 155–188. https://doi.org/10.1558/jmea.v13i2.155.

Spatafora, F., 2005. Ustica e le rotte tirreniche. Il Villaggio dei Faraglioni (campagne di scavo 2003-2004). In: Les Lingots peau-de-boeuf et la navigation en Mediterranee Centrale, Actes du II Colloque international (Lucciana, Mariana 15-18 settembre 2005), pp. 133–141.

Spatafora, F., 2016. Tra mare e terra: la preistoria di Ustica e il villaggio dei Faraglioni in, in Ubi minor… Le isole minori del Mediterraneo centrale dal Neolitico ai primi contatti coloniali (a cura di A.Cazzella, A.Guidi, F.Nomi), Scienze dell’Antichità, 22, Fascicolo, 2, pp. 315–326.

Spatafora, F., Mannino, G., Soprintendenza, Palermo, Ambientali, Peri Beni Culturali e, 2008. Ustica: guida breve. (Regione Siciliana). Assessorato Regionale dei Beni Culturali Ambientali e della Pubblica Istruzione.

Speciale, C., Freund, K.P., de Vita, S., Larosa, N., Forgia, V., Battaglia, G., Tykot, R.H., Vassallo, S., 2021a. Obsidian from the Site of Piano Dei Cardoni, Ustica: preliminary results on the first Occupation of the Island. Open Archaeol. 7, 273–290. https://doi.org/10.1515/opar-2020-0140.

Speciale, C., Montana, G., Mentesana, R., Forgia, V., Mantia, F., Battaglia, G., Di Vito, M. A., Vassallo, S., de Vita, S., 2021b. Materials and tools across volcanoes: exploitation of georesources in Piano dei Cardoni (Ustica, Italy) during prehistory. Ann. Geophys. 64 (5), VO552. https://doi.org/10.4401/ag-8684.

Tykot, R.H., Martin, F.F., 2020. Analysis by pXRF of prehistoric obsidian artifacts from several sites on Ustica (Italy): Long-distance open-water distribution from multiple

island sources during the Neolithic and Bronze ages. Open Archaeol. 6 (1), 348–392. https://doi.org/10.1515/opar-2020-0118.
Voza, G., 1972. Thapsos, primi risultati delle più recenti scoperte. In: Atti della XIV Riunione Scientifica Istituto Italiano Preistoria e Protostoria, Firenze, 1972, pp. 175–205.
Yilmaz, S., Balkaya, Ç., Cakmak, O., Oksum, E., 2019. GPR and ERT explorations at the archaeological site of Kılıç village (Isparta, SW Turkey). J. Appl. Geophys. 170, 103859.